We are IntechOpen,
the world's leading publisher of
Open Access books
Built by scientists, for scientists

4,800
Open access books available

122,000
International authors and editors

135M
Downloads

Our authors are among the

154
Countries delivered to

TOP 1%
most cited scientists

12.2%
Contributors from top 500 universities

CLARIVATE ANALYTICS
BOOK
CITATION
INDEX
INDEXED

WEB OF SCIENCE™

Selection of our books indexed in the Book Citation Index
in Web of Science™ Core Collection (BKCI)

Interested in publishing with us?
Contact book.department@intechopen.com

Numbers displayed above are based on latest data collected.
For more information visit www.intechopen.com

Indentation and Fracture of Hybrid Sol-Gel Silica Films

Bruno A. Latella, Michael V. Swain and Michel Ignat

Additional information is available at the end of the chapter

1. Introduction

Organic-inorganic hybrid thin films fabricated using sol-gel processing have many compelling properties that render them quite attractive for many applications, including optics, electronics, sensors and corrosion and scratch resistant films (Haas & Wolter, 1999; Sanchez et al., 2005). Organic-inorganic hybrid network materials have received much interest as transparent functional coatings on polymer substrates (Haas & Wolter, 1999; Haas et al., 1999a) and barrier coatings on metals (Metroke et al., 2001). Compared to glass, polymers such as polycarbonate (PC) and glycol bis(allyl carbonate) (CR-39) exhibit several advantageous physical and mechanical properties, such as high impact resistance and reduced weight, but also have the significant disadvantage of higher refractive index resulting in greater surface reflections as well as a much lower tolerance to abrasion. These drawbacks have limited their exploitation as a replacement to glass, especially for ophthalmic lenses where reflections and scratches on lenses can significantly obscure vision. The incorporation of a film or coating on glass or polymer can have immense benefits as is the case in the eyewear industry where several layers are deposited on polymer substrates to overcome substrate limitations (Samson, 1996; Schottner, 2001). By controlling the chemistry of the organic component incorporated in hybrid films, the physical and mechanical properties can be readily adjusted to realise specific attributes such as scratch resistance. Yet a vital reliability issue for film-on-substrate systems is the intrinsic mechanical properties of the film and adhesion to the substrate (Ignat et al., 1999).

In order to achieve good scratch resistance, two properties need to be optimised: *adhesion* of the film to the substrate and film *hardness*. In hybrid films, hardness is provided by the inorganic ceramic phase or from nano-particle inclusions. Not as much attention has been paid to adhesion behaviour of these hybrid film-substrate systems although enhancements in adhesion may be achieved using organic materials, which are softer and generally more

flexible as compared to the inorganic, which are typically harder and more brittle. Hence, hybrid coatings are considered extremely versatile given the combination of these two very different material characteristics for films to be tailored to achieve a range of functional responses. Accordingly, in this chapter nanoindentation and tensile testing are surveyed as tools to characterise film properties, fracture behaviour and adhesion to the underlying substrate of a variety of model hybrid films. This begins with an overview of hybrid sol-gel film processing. The key principles of nanoindentation focussing on spherical indentation to examine elastic-plastic response and creep behaviour are then outlined. Finally, tensile testing and the mechanics for ascertaining film fracture properties and film-substrate adhesion are described along with specific examples to illustrate the combined power of the techniques.

2. Hybrid sol-gel films – Overview

A hybrid material is any organic-inorganic system in which at least one of the components, organic or inorganic, is present with a size scaling from tenths to tens of nanometres. Components used to make hybrids can be molecules, oligomers or polymers, aggregates and even particles. Therefore they can be considered as nanocomposites at the molecular scale. Schmidt (Schmidt, 1985) and Wilkes (Wen & Wilkes, 1996) have been widely credited with pioneering the research into organic-inorganic hybrids using the sol-gel process. They both showed that an organic polymer can be chemically bonded to an inorganic oxide network to form a new type of polymer. Schmidt named his hybrid material "ORMOSILs" (for ORganically MOdified SILicates) or "ORMOCERs" (for ORganically MOdified CERamics) while Wilkes named his materials "CERAMERs" (for CERAmic polyMERS).

Hybrid materials can be classified by their chemical composition or by the nature of the chemical interactions (Sanchez et al., 2005). Reactive monomers linked through covalent chemical bonds to the inorganic network react in the wet film through organic cross-linking reactions. Depending on the chemical nature of the reactive species (vinyl, epoxy, acrylic, etc.), various organic network types can be formed. They can be classified by four compositional parameters (Haas et al., 1999b): (i) Type I: nonorganically modified Si alkoxides; (ii) Type II: heterometal alkoxides; (iii) Type III: organically modified reactive Si alkoxides; and (iv) Type IV: functional organically modified Si alkoxides.

The adaptation of materials for special applications is mainly determined through the use of these four structural elements and the conditions for forming inorganic and organic networks (Mackenzie & Bescher, 1998; Mackenzie & Bescher, 2003). For example, the amount of inorganic structures and the extent of organic cross-linking can have a dramatic influence on the mechanical properties (Mackenzie & Bescher, 2000) as will be shown in section 5. A high inorganic content leads to stiff but brittle materials. Hardness combined with elasticity is realised by using inorganic structures with a certain amount of organic cross-linking (Mammeri et al., 2005).
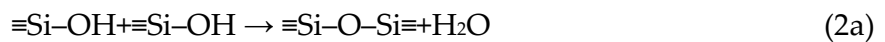
Sol-gel technology is used to produce hybrid coatings because: (i) it allows the formation of hybrid structure at temperatures below 150 °C; (ii) it is attractive for coating polymers which

have melting points between 150°C and 300°C; (iii) coatings can easily be produced by dip or spin coating; (iv) the technology is simple to implement on a large scale and it is cheap; and (v) ceramic, metal and polymer substrates can be easily coated. For a comprehensive understanding of sol-gel technology and hybrid film processing see refs (Brinker & Scherrer, 1990; Haas et al., 1999b; Letailleur et al., 2011).

The general processing scheme for hybrids is shown in Figure 1. The reaction is divided into hydrolysis and polycondensation (Brinker & Scherrer, 1990). The hydrolysis reaction induces the substitution of OR groups linked to silicon by silanol Si-OH groups:

$$\equiv Si–OR+H_2O \rightarrow \ \equiv Si-OH+ROH \tag{1}$$
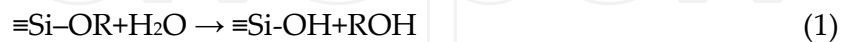
These chemical species may react together to form Si-O-Si (siloxane) bonds which lead to the silica network formation. The polycondensation equations are:

$$\equiv Si–OH+\equiv Si–OH \rightarrow \ \equiv Si–O–Si\equiv+H_2O \tag{2a}$$

$$\equiv Si–OH+\equiv Si–OR \rightarrow \ \equiv Si–O–Si\equiv+ROH \tag{2b}$$

Polycondensation leads to the formation of a sol which can be deposited on a substrate using spin, spray, flow or dip coating. When the sol is applied on a substrate, the wet film can be further cross-linked thermally or by using UV/IR radiation to evaporate the water and alcohol remaining in the pores and increase the bonding to the substrate.

3. Nanoindentation

Nanoindentation is an exceptionally versatile technique and is ideal for quantifying mechanical properties of materials at the sub-micron scale (Oliver & Pharr, 1992; Fischer-Cripps, 2002). The growing need to study the mechanical properties of small volumes, thin films and surface treated materials has seen dramatic developments in sub-micron indentation testing and instrumentation capable of loads down to tens of micro-newtons to produce nanometre size indentations. The two basic properties readily obtained are hardness (H) and Young's modulus (E).

3.1. Spherical versus sharp indentation

Indenters can generally be classed into two categories: *sharp* (pointed) or *blunt* (spherical). The fundamental difference between the indentation of a pointed indenter and a spherical indenter in a material is that the pointed indenter induces an immediate plastic response at the point of first contact with the material while the spherical indenter induces an elastic-plastic response. Examples of these differences on the resultant load-displacement curves of a silica glass (E = 70 GPa, ν= 0.17) using four typical indenter types with a maximum load of 1 mN are shown in Figure 2. In these tests only the spherical indenter displayed a completely reversible elastic contact.
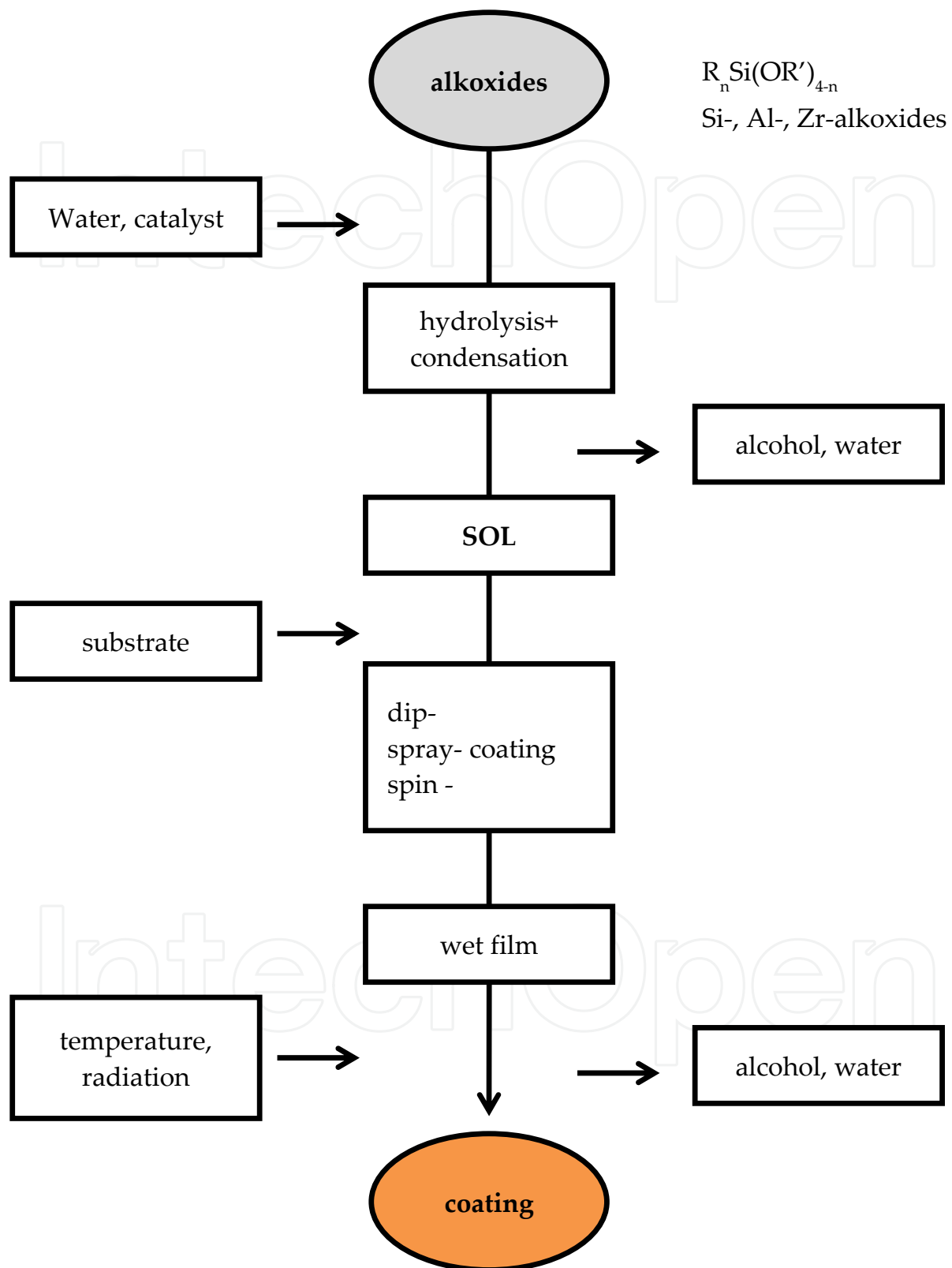
Figure 1. Ormocer® processing for coatings [Redrawn from ref (Haas et al., 1999b) with permission from Elsevier].
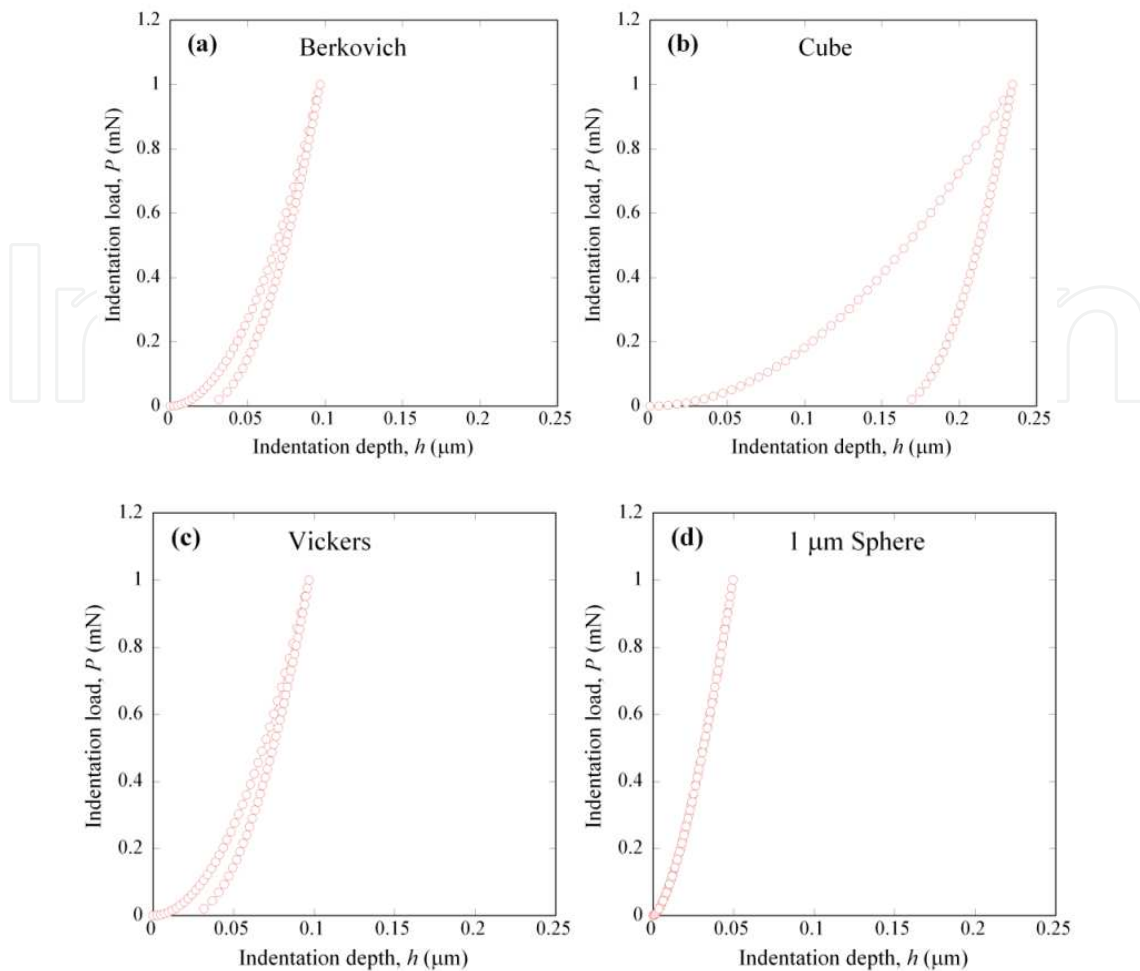
Figure 2. Load versus depth profiles for silica glass (E = 70 GPa, υ = 0.17) at 1 mN maximum load for diamond indenter types: (a) Berkovich, (b) cube-corner, (c) Vickers and (d) 1 μm sphere.

3.1.1. Pointed indenters

Pointed indenters used in nanoindentation are made of diamond and are either Berkovich, Vickers, Knoop or cube-corner geometry (Fischer-Cripps, 2002). The radius of the indenter tip is significantly smaller than that used for microhardness testing. The Berkovich indenter is often favoured as its three-face pyramid geometry is much easier to grind to a sharp point compared to the four-face pyramid geometry of Vickers and Knoop. The cube-corner indenter is now used widely for initiating cracks and therefore facilitates fracture toughness measurements (Fischer-Cripps, 2002; Volinsky et al., 2003). Stresses beneath pointed indenter tips are very high and in theory are infinite at the point of contact with an elastic body. In reality the tip is always a little blunt as no indenter is ideally sharp. Berkovich indenters can be used as a spherical tip for ultra-low contact loading. For pointed indenters the distribution of stress in a homogeneous material remains constant regardless of the penetration depth of the indenter. The mean contact pressure or indentation hardness and the average strain are constant and are the reasons why it is good for hardness determinations. The average or equivalent strain is only dependent on the indenter angle.

3.1.2. Spherical indenters

With spherical indenters the stresses are symmetrical and, unlike pointer indenters have no preferred direction; this means that the orientation of the indenter plays no role in the determination of the properties of crystals or anisotropic materials. The primary use of a spherical indenter is to reveal information on the transition from elastic to elastic-plastic or elastic-brittle behaviour in materials. During the initial stage of penetration into the surface the contact zone is deformed elastically but at larger loads a transition to elastic-plastic occurs and the average strain increases with the depth of penetration as the depth of contact area grows faster than the indenter radius. Therefore, it is possible to construct diagrams of indentation stress versus strain (He et al., 2008). As opposed to pointed indenters the strain increases with increasing depth of penetration for spherical indenters. For thin, soft and compliant (low *H* and *E)* coatings spherical indentation is useful for characterising film behaviour particularly the elastic to plastic transition and viscoelastic properties (Oyen, 2006; Latella et al., 2008a) and for hard coatings the evolution in damage (Haq et al., 2010). For these reasons the discussion and mechanics that follows is restricted to spherical indentation.

3.2. Measurement of hardness and elastic modulus

Since the pioneering work of Hertz (Hertz, 1896) the nature of contact damage that forms in a brittle solid loaded with a sphere has been extensively studied (Lawn, 1998). For spherical indentation of a rigid sphere into a specimen at low loads the Hertz equation for elastic loading is:

$$P = \frac{3}{4} E_{eff} R^{1/2} h_e^{3/2} \qquad (3)$$

where *R* is the sphere radius, h_e the elastic penetration depth and E_{eff} is the effective elastic modulus given by:

$$\frac{1}{E_{eff}} = \frac{1 - v_m^2}{E_m} + \frac{1 - v_i^2}{E_i} \qquad (4)$$

where *E* is Young's modulus, v is Poisson's ratio and the subscript *i* denotes the indenter material and *m* the sample. For higher loading elastic and plastic deformations occur within the specimen material. At full load the depth of penetration of the sphere below the original specimen surface is h_t. During unloading the response is elastic and at complete unload a residual impression depth, h_r is left. If the load is then re-applied, the loading is again elastic through the distance $h_e = h_t - h_r$, according to equation 3.

There are two possible approaches with spherical indentation, the continuous load-unload cycle (Oliver & Pharr, 1992) or the load-partial unload cycle (Field & Swain, 1993; Field & Swain, 1995). The continuous load–unload sequence for spherical indenters is essentially the same as the continuous load-unload sequence used for pointed indenters. However, the continuous load-unload data for spherical indenters is usually more difficult to

analyse than it is for pointed indenters due to the changing strain and the need to determine and separate the elastic and plastic components of the load-displacement data. This difficulty is overcome by the load-partial unload technique which leads to a relatively simple expression for materials exhibiting permanent plastic deformation during indentation.

The continuous load-unload cycle (Oliver & Pharr, 1992) uses multiple points from the maximum load to determine the slope of the initial unloading portion of a single-cycle load-displacement curve. In contrast for the load partial-unload technique (Field & Swain, 1993; Field & Swain, 1995) typically a 50% unload from the maximum load for multiple increments of loading is used. From the tests the effective Young's modulus can be determined:

$$E = \frac{3P}{4ah_e} \tag{5}$$

where a is the contact radius $a = \sqrt{2Rh_p - h_p^2}$

with R the sphere radius and h_p the plastic penetration depth or depth of the circle of contact, h_e is the elastic penetration depth ($h_e = h_t - h_r$) with h_t the maximum penetration depth at full load P and h_r the residual depth of the impression upon unloading. The depth of the residual impression is obtained from the measurement of load P_s and penetration h_s at partial unload from the higher load P_t and forming the ratio of the elastic displacements:

$$h_r = \frac{h_s(P_t/P_s)^{2/3} - h_t}{(P_t/P_s)^{2/3} - 1} \tag{6}$$

Similarly the hardness, H, or contact pressure is given as:

$$H = \frac{P}{A} \tag{7}$$

where $A = \pi a^2 = 2\pi Rh_p - \pi h_p^2$.

The strain increases with indentation impression depth, and an appropriate equivalent expression is:

$$\epsilon = 0.2\, a/R \tag{8}$$

Hence plotting H versus a/R is the contact stress-strain curve. The contact area and contact pressure are calculated for every partial unloading step and provides a measure of hardness and modulus as a function of depth of penetration of materials whose properties vary with penetration.

3.3. Indentation creep

The discussion above has assumed time-independent material behaviour but this is not always the case for materials such as polymers which exhibit time-dependent deformation

under loading. The time-dependent deformation can be described in terms of creep and stress relaxation. Creep is the time-dependent deformation that occurs under constant stress while stress relaxation is the stress response under constant strain. The discussion in this chapter will be restricted to creep.

3.3.1. Methodology

As with conventional creep testing of structural materials, nanoindentation creep testing provides an accurate measure of indentation depth changes as a function of time (Lucas & Oliver, 1999; Oyen, 2006). The method is best performed using fast loading (high strain rate) to the desired load, held at the load for a predetermined time and then unloaded. If a slow step loading is performed then differences in the creep deformation and creep parameters are expected purely due to the effect of strain rate.

3.3.2. Models

It is well known that the organic component in hybrid films exhibits polymeric-like behaviour. Hence the creep in these films can be readily modelled using a combination of springs and dashpots (Bland, 1960; Fischer-Cripps, 2004). The starting point is that the elastic deformation in a material can be described by a *spring* that responds to an applied stress (Hooke's law):

$$\sigma = E\epsilon \tag{9}$$

With the added influence of time dependency the *dashpot* represents a Newtonian viscous substance as follows:

$$\sigma = \eta \left(\frac{d\epsilon}{dt}\right) \tag{10}$$

Therefore by connecting springs and dashpots together in series and parallel combinations various models can be devised (Bland, 1960). The phenomenological spring dashpot models used widely for analysing indentation creep are illustrated in Figure 3.

Lee and Radok (Lee & Radok, 1960) addressed the problem for indentation of a smooth rigid sphere on a semi-infinite viscoelastic plane to determine the relation between indentation force and displacement. The solution is based on viscoelastic extensions of Hertzian contact (see equation 3) by combining the elastic and dissipative components (Bland, 1960; Kumar & Narasimhan, 2004):

$$h^{3/2}(t) = \frac{a^3}{R^{3/2}} = \frac{3}{4} \frac{P}{R^{1/2}} \left[\frac{1}{E_s} + \frac{t}{\eta_s} + \psi(t) \right] \tag{11}$$

where E_s, η_s and $\psi(t)$ are the instantaneous elastic modulus, the long term viscous flow constant and the creep response function of the form $\psi(t) = 1 - e^{-Et/\eta}$.
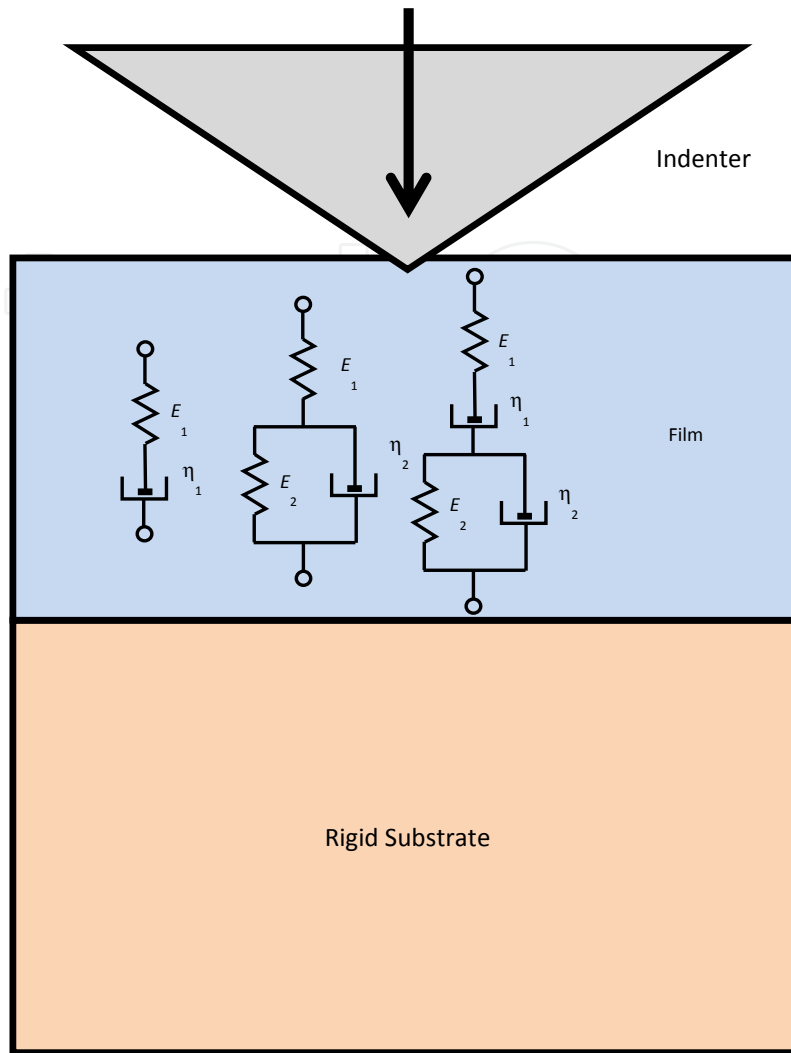
Figure 3. Schematic illustration of spring-dashpot models for indentation on film-substrate system. From left to right: Maxwell, three-element and four-element (Bürger) models.

For the Maxwell model it can be shown that:

$$\frac{d\varepsilon}{dt} = \frac{1}{E_1}\frac{d\sigma}{dt} + \frac{\sigma}{\eta_1} \tag{12}$$

where ε is the strain and σ is the stress.

So that the time-dependent depth of penetration for a spherical indenter in this case is:

$$h^{3/2}(t) = \frac{3}{4}\frac{P_{max}}{R^{1/2}}\left[\frac{1}{E_1} + \frac{t}{\eta_1}\right] \tag{13}$$

Likewise, for the standard linear solid (three-element) model the constitutive relation is:

$$\left(1 + \frac{E_1}{E_2}\right)\sigma + \left(\frac{\eta_1}{E_2}\right)\frac{d\sigma}{dt} = E_1\varepsilon + \eta\frac{d\varepsilon}{dt} \tag{14}$$

and:

$$h^{3/2}(t) = \frac{3}{4} \frac{P_{max}}{R^{1/2}} \left[\frac{1}{E_1} + \frac{1}{E_2}(1 - e^{-E_2 t/\eta_1}) \right] \qquad (15)$$

The constitutive equation for the four-element model is:

$$\sigma + \left[\frac{\eta_1}{E_1} + \frac{\eta_1}{E_2} + \frac{\eta_2}{E_2} \right] \frac{d\sigma}{dt} + \left[\frac{\eta_1 \eta_2}{E_1 E_2} \right] \frac{d^2\sigma}{dt^2} = \eta_1 \frac{d\varepsilon}{dt} + \left[\frac{\eta_1 \eta_2}{E_2} \right] \frac{d^2\varepsilon}{dt^2} \qquad (16)$$

and:

$$h^{3/2}(t) = \frac{3}{4} \frac{P_{max}}{R^{1/2}} \left[\frac{1}{E_1} + \frac{t}{\eta_1} + \frac{1}{E_2}(1 - e^{-E_2 t/\eta_2}) \right] \qquad (17)$$

Equations 13, 15 and 17 can then be used to obtain best fits to the experimental data by systematically adjusting the fitting parameters (E_1, E_2, η_1, η_2) using an iterative procedure with the Levenberg–Marquardt algorithm. The starting values for the fitting parameters are based on nanoindentation results and a refinement of estimates for the other parameters to achieve fits with correlation coefficient $R^2 > 0.95$. Similarly creep in thin films has been analysed using logarithmic relations (Berthoud et al., 1999; Chudoba & Richter, 2001; Beake, 2006) such as:

$$h(t) = A + B \ln \left[(Ct) + 1 \right] \qquad (18)$$

where A, B and C are fitting constants and t is the time. This equation does not give E and η but the coefficient B is defined as an extent term and C as a rate term for deformation (Beake, 2006).

4. Microtensile testing

4.1. Background

Characterising the cracking evolution, debonding behaviour and adhesion performance of thin films subject to external applied stresses is an important aspect in materials selection for specific applications. As a complement to nanoindentation testing, micro-mechanical tensile testing is valuable in elucidating the critical conditions for cracking and debonding of thin brittle films on ductile substrates (Ignat, 1996; Ignat et al., 1999). These types of experiments have been shown to offer insights into evaluating interfacial adhesion of thin films and multilayered structures (Agrawal & Raj, 1989; Filiaggi et al., 1996; Scafidi & Ignat, 1998; Wang et al., 1998; Harry et al., 2000; Latella et al., 2007a; Roest et al., 2011).

In this type of test a film is deposited on a tensile coupon, which can then be pulled in a universal testing machine or a specialized device and the surface can be viewed with an optical microscope or in a scanning electron microscope. Brittle coatings produce parallel

cracks on ductile substrates when uniaxially stressed perpendicular to the tensile axis – see section 5 for examples. These cracks generally extend through the thickness of the coating and along the width of the sample and increase in number with additional elongation, leading to a decrease in the crack spacing. For some systems, cracks may also be accompanied by localized delamination of the coating from the substrate. Eventually, delamination of the coating signals the end of the lifetime of the coated system. For more compliant films, cracking can be irregular and film debonding reduced substantially.

Tensile testing is advantageous in that the stress field is uniform along the gauge length of the sample and relatively small specimens can be used. Similarly, using optical or scanning electron microscopy (SEM) to view the damage *in-situ* during loading reveals fracture and film failure mechanisms (Ignat et al., 1999; Latella et al., 2004; Latella et al., 2007b). The only prerequisite for this type of test is that for analysis of the coating behaviour, the residual stress, and Young's modulus of the coating are required by other means, such as from substrate curvature measurements and nanoindentation, respectively.

4.2. Mechanics

It is recognised that cracking of a film and its detachment from an underlying substrate are controlled by the intensity of the stored elastic energy. For a thin film subjected to an in plane isotropic stress, the elastic stored energy is:

$$U = \frac{1-\nu_f}{E_f}\sigma_f{}^2 t \tag{19}$$

where σ_f is the normal stress in the film, ν_f, E_f and t are the Poisson's ratio, Young's modulus and thickness of the film, respectively. Hence a film under tension will crack when U equals the films cracking energy and for a film under compression will delaminate when U equals the interfacial cracking energy. Accordingly the mechanical stability of the film depends on its strength and fracture toughness and adhesion behaviour. Micromechanical tensile testing is useful because these key material parameters can be readily studied.

For a film-substrate system that is strained in tension the requirement is to determine the instant of first cracking in the film, which corresponds to a strain ε_c. Using Young's modulus of the film (E_f) the critical stress, σ_c, for cracking or film strength is calculated as follows:

$$\sigma_c = \epsilon_c E_f + \sigma_r \tag{20}$$

where σ_r is the residual stress in the film.

The fracture energy of the coating is obtained from (Hu & Evans, 1989):

$$\gamma_f = \frac{\sigma_c^2 t}{E_f}\left(\pi g(\alpha) + \frac{\sigma_c}{\sqrt{3}\sigma_y}\right) \tag{21}$$

where γ_f is the fracture energy, t is the thickness of the film, σ_y is the yield stress of the substrate and α is Dundar's parameter $\alpha = (E_f - E_s)/(E_f + E_s)$, where E_s is Young's modulus of the substrate and $g(\alpha)$ is obtained from (Beuth & Klingbeil, 1996).

Adhesion of the film to the substrate is determined by the measurement of the interfacial fracture energy. The instant of first debonding of the film during tensile loading corresponds to a strain ϵ_d. The apparent interfacial fracture energy is given by (Hu & Evans, 1989):

$$\gamma_i = \frac{E_f}{2} t \epsilon_d^2 \qquad (22)$$

5. Experimental studies

5.1. Case study 1 – Different length and functionality of organic

Sol-gel coating solutions were prepared by adding a 0.01 M solution of nitric acid (HNO_3) to equimolar mixtures of tetraethylorthosilicate (TEOS) and selected alkyltriethoxysilanes in dry ethanol with equivalent SiO_2 concentrations of 5 wt%, specifically, methyltrimethoxysilane (MTMS), vinyltrimethoxysilane (VTMS) and 3-glycidoxypropyltrimethoxysilane (GTMS). GTMS is a low cost and readily available commercial compound and is of major interest as it is widely used for coatings in optical and anti-corrosion applications. The molecule has a long organic chain composed of seven carbons and an epoxy ring polymerisable at its end group.

A solution of 100% TEOS was also prepared as the control. A water-to-alkoxide ratio of 10 was used in all cases and the solutions were aged at room temperature for 24 h before use. The chemical structures of the organic constituents are given in (Atanacio et al., 2005). Thin film coatings were deposited on silicon wafers (25.4 mm diameter; thickness, 0.5 mm; single sided polished) and polished stainless steel coupons by spin coating at 5000 rpm for two minutes. The coated specimens were then allowed to dry for 24 h at 60°C. The coatings produced were transparent and amorphous in nature and given the following designations: (i) TEOS (thickness, t = 270 nm), (ii) MTMS (t = 280 nm), (iii) VTMS (t = 250 nm) and (iv) GTMS (t = 620 nm).

Figure 4 shows full cycle spherical indentation load-displacement curves for the films with a 30 s dwell at 1 mN maximum load. The key features to note from the load-displacement curves are differences in the maximum penetration depth, the increase in penetration for the 30 s dwell at peak load and the recovery behaviour of the films during the unloading cycle. The TEOS film initially displays elastic behaviour, which is then followed by small deviations from the ideal elastic behaviour based on computation of simulated load-depth curves. The MTMS and VTMS films show similar trends, although with a much greater degree of compliance, with their response curves displaced to the right. The GTMS film, on loading, displays a dramatic increase in penetration far exceeding those of the other films, and even more striking on unloading, is the dramatic recovery from 0.4 mN to complete unload of approximately 340 nm, not evident in the other films and indicative of polymer-like behaviour. This is most likely due to viscoelastic flow and relaxation processes, as there is little permanent deformation with the creep and recovery being almost reversible. The TEOS film shows the least amount of deformation, attributable to the predominantly silica comprised network providing rigidity and hence less molecular movement under constant load. The MTMS and VTMS are intermediate and the GTMS film shows the greatest

deformation. A study of silica nano-particle filled hybrid films on glass showed similar mechanical responses (Malzbender et al., 2002).
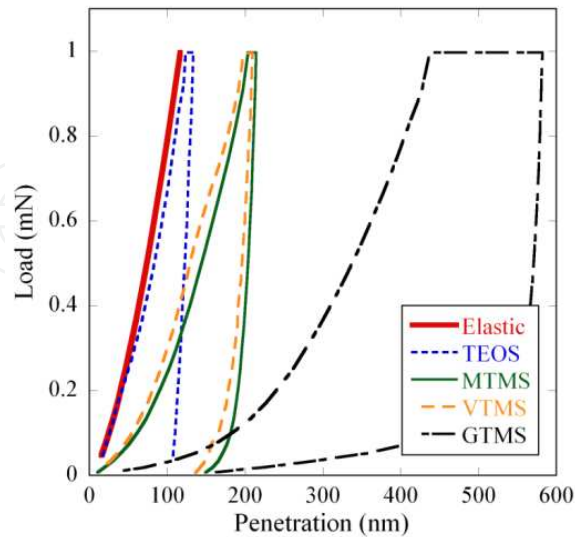
Figure 4. Load-displacement response for spherical indentation of the four coatings on silicon. The bold red curve denoted Elastic is the calculated Hertzian elastic response for the TEOS film [Redrawn from ref (Latella et al., 2003)].

The derived indentation stress-strain curves of the films from the load-partial unload method are shown in Figure 5. Again the results show the increasing deviation in mechanical response of the films from nominally elastic-brittle for TEOS (E = 18.8 GPa; H = 0.6 GPa), intermediate for MTMS (E = 5.6 GPa; H = 0.3 GPa) and VTMS (E = 4.8 GPa; H = 0.3 GPa) films to elastic-plastic for GTMS (E = 0.9 GPa; H = 0.15 GPa). The curves indicate that the addition of organics leads to a decrease in Young's modulus and a greater tendency for energy absorbing behaviour particularly in GTMS to minimise damage under contact loading. The transition is analogous to that observed in porous hydroxyapatites (He et al., 2008).
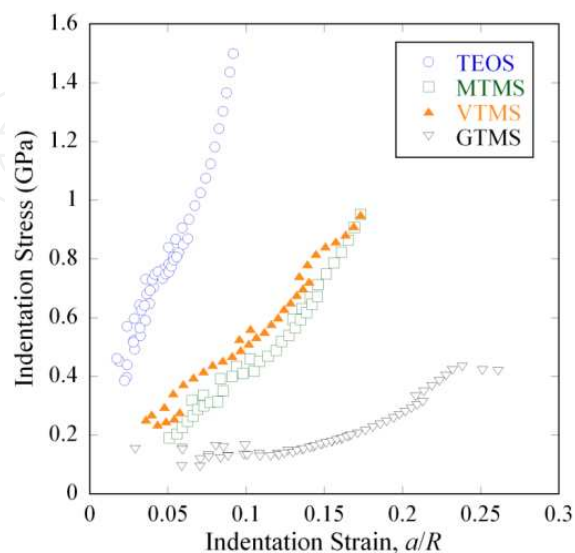
Figure 5. Indentation stress-strain behaviour of the four films.

The results concerning the influence of chain length and functionality of the organic precursors introduced in the inorganic network on the mechanical properties are linked to the structure and the network. By introducing different organic chain lengths dramatic modifications in the connectivity of the network are expected. For pure inorganic silica coatings the structure is dense but with the addition of a small chained organic component the short-range network is significantly modified. For example when MTMS (1 carbon chain length) is introduced, some silica domains may be formed but the structure is not dramatically modified suggesting that the silica domains are still closely grouped. However, the modification that occurs leads to a discernible difference in the mechanical properties compared to the pure inorganic coating (TEOS). By comparison when GTMS (7 carbon chain length) is introduced the mechanical properties are reduced further. In this case, it is thought that the longer GTMS chain creates larger gaps between the silica-rich domains, which are much further apart. This result in the connectivity of the network to be significantly lowered compared to a pure inorganic network.

To complement the indentation testing results, similar composition films deposited on stainless steel dogbones were uniaxially loaded in tension at a rate of 0.003 mm/s using a high-stiffness mechanical testing device (Ignat et al., 1999) positioned directly under the objective lens of an optical microscope (Zeiss Axioplan) at a fixed magnification. This allowed direct observation of crack initiation and evolution and debonding of the thin films on the steel specimens (see section 4). The applied load and the imposed displacement were recorded during the tests and optical images were captured at designated points as shown in the example in Figure 6 for the base TEOS film. Higher magnification views of the four films were obtained on carbon coated samples using SEM (JEOL 6300).
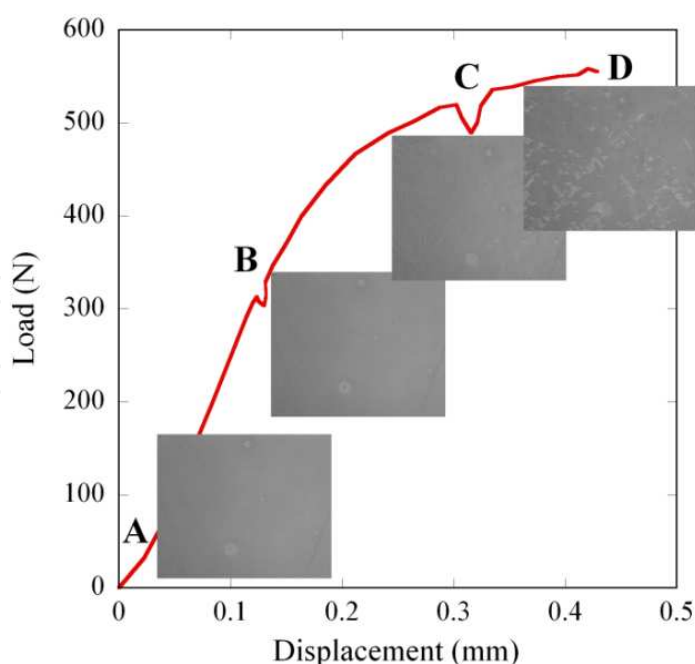

Figure 6. Load-displacement curve from tensile test of the TEOS coated stainless steel. Inset images at points A (0 N), B (320 N), C (520 N) and D (560 N) correspond to the specimen surface during loading (field of view in each image is 400 μm) [After (Latella et al., 2003)].

Figure 7 shows SEM images of the four thin film coatings after tensile testing. The baseline TEOS film (Fig. 7(a)) displays characteristic brittle behaviour with cracks at about a 90° angle to the loading direction (transverse cracking) and normal to the interface. Delamination of the coating is obvious and buckling occurs readily in these areas. The MTMS film (Fig. 7(b)) also showed cracking but it was more irregular and there was a great deal of debonding. The VTMS film (Fig. 7(c)) exhibited less debonding than MTMS but it had transverse cracking with a similar inter-cracking distance. By contrast the longer-chained GTMS film (Fig. 7(d)) resulted in excellent substrate–film bonding with little cracking and decohesion of the film. The same type of cracking and debonding is observed in related tensile testing of these films on copper substrates – see ref (Atanacio et al., 2005) and later in section 5.2.

Clearly the size of the organic chain has a dramatic influence on the mechanical response of the films in contrast to the relatively brittle baseline TEOS film (Schmidt 1985). The reduction in Young's modulus and the greater resistance to cracking and debonding of the films with increasing organic-modifier showed that the films can be tailored by simple manipulation of the sol-gel chemistry. The larger chained organic component results in a structure which is not unlike a polymer, as is the case in the GTMS film, which minimises film cracking. The mechanical property results suggest that there is an important rearrangement of the organic modifier links in these hybrids that controls the deformation, hence the transition to semi-brittle or viscoelastic response (Latella et al., 2003; Atanacio et al., 2005). Similar behaviour has been observed in bulk samples made from TEOS and polydimethylsiloxane (PDMS) (Mackenzie, 1994). Mackenzie demonstrated that the mechanical properties could vary from being hard and brittle to rubbery and soft, depending on the ratio of organic to inorganic constituents. Samples were found to retain a rubbery nature even when the inorganic constituent was in excess of 70 wt%. However, when the PDMS content was less than 10 wt%, the sample became brittle. Mackenzie proposed that small concentrations of PDMS react in solution to form gels with a porous three dimensional network still dominated by the Si-O-Si linkages. However, as the PDMS content increases, the structure is characterised more by silicon clusters linked with flexible chains of PDMS.
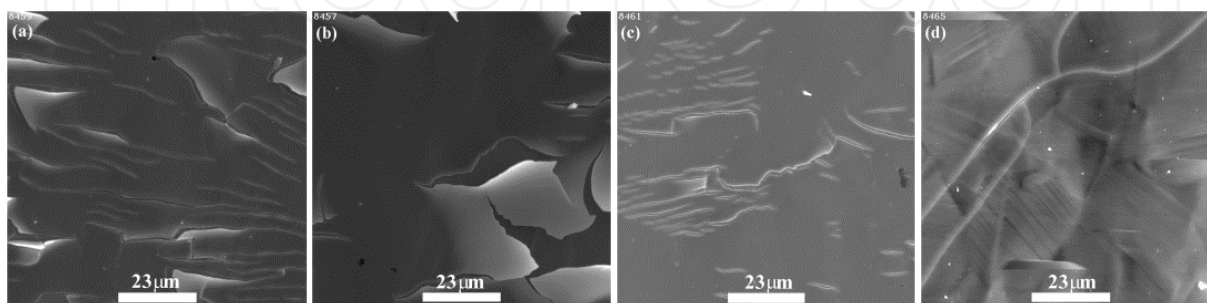

Figure 7. SEM images of the films: (a) TEOS, (b) MTMS, (c) VTMS and (d) GTMS on stainless steel substrates after tensile loading [from ref (Latella et al., 2003)]. Heterogeneous cracking with marked debonding is obvious in (a) and (b). Tensile axis is vertical in these images.

5.2. Case study 2 – Different amount of organic

In this study the effect of increasing amount of GTMS was examined for films deposited on copper sheet. The Cu sheet was cut into samples of about 40 mm in length and 20 mm width and as tensile dogbones (12 mm gauge length, 3 mm width at the gauge and 1 mm thickness). The samples were polished to a 1 µm finish then cleaned in soap solution and ethanol and then dried. Sol-gel solutions were prepared by adding a 0.01 M solution of HNO_3 to (i) TEOS and (ii) a mixture of 25%, 50% or 75% of the organic GTMS and TEOS (75%, 50% and 25%) in ethanol. Each solution contained an equivalent SiO_2 concentration of 5 wt% and a water-to-alkoxide mole ratio of 10. The solutions were spin coated on the copper samples and then dried at 60°C for 24 h in a clean room environment. Thickness of the coatings was determined using spectroscopic ellipsometry (Sopra GES). The coatings produced were transparent and amorphous in nature and given the following designations based on the precursors used: (i) TEOS (thickness, t = 190 nm), (ii) 25% GTMS (t = 290 nm), (iii) 50% GTMS (t = 450 nm) and (iv) 75% GTMS (t = 600 nm).

The indentation load-displacement curves (P_{max} = 1 mN) are shown in Figure 8 for the TEOS and the 25%, 50% and 75% GTMS films deposited on the copper substrates using a nominal 1 µm spherical indenter. A 10 s hold at maximum load was used to provide a qualitative assessment of creep. The load-displacement curve of the TEOS coating is typical of an elastic-brittle material, showing initially elastic loading then elastic-plastic behaviour up to maximum load. The GTMS films show an increasing tendency, with higher organic, for greater penetration on loading indicative of soft and compliant coatings. It is important to note that the TEOS film is thin and Cu is much softer than Si (*cf.* with Figure 4) so plastic deformation of the substrate is more prevalent. Also with the increased % GTMS the films are progressively thicker and softer so now most of the deformation is in the film rather than in the substrate. At peak load, there was detectable creep, particularly for the 75% GTMS, and then on unloading there was recovery back to a low residual penetration, symptomatic of viscoelastic behaviour. A better approach here would be to hold at low load to quantify the recovery with time to give a clearer indication of viscoelastic response (He & Swain, 2009).

The hardness, H, and Young's modulus, E, of the three GTMS films, determined using the load partial unload technique (see section 3.2), as a function of percentage organic is given in Figure 9. The hatched boxes at the left are for the baseline silica film (100% TEOS): H = 2.15 GPa and E = 55 GPa. Compared to the TEOS film there was a large drop in both hardness and Young's modulus of the GTMS films, which decreased with increasing organic, confirming the observations of the load-displacement curves in Figure 8. Clearly, with the introduction of the long-chained organic there is a prominent drop in the mechanical properties and evidence of a change from elastic-brittle to viscoelastic behaviour in the sol-gel matrix due to the influence of organic species and its modifying ability on the inorganic network structure (Metroke et al., 2001; Atanacio et al., 2005). The H and E values are comparable to that for bulk GTMS hybrids (Innocenzi et al., 2001) and comparisons with a myriad of hybrid coatings can be found in (Mammeri et al., 2005).
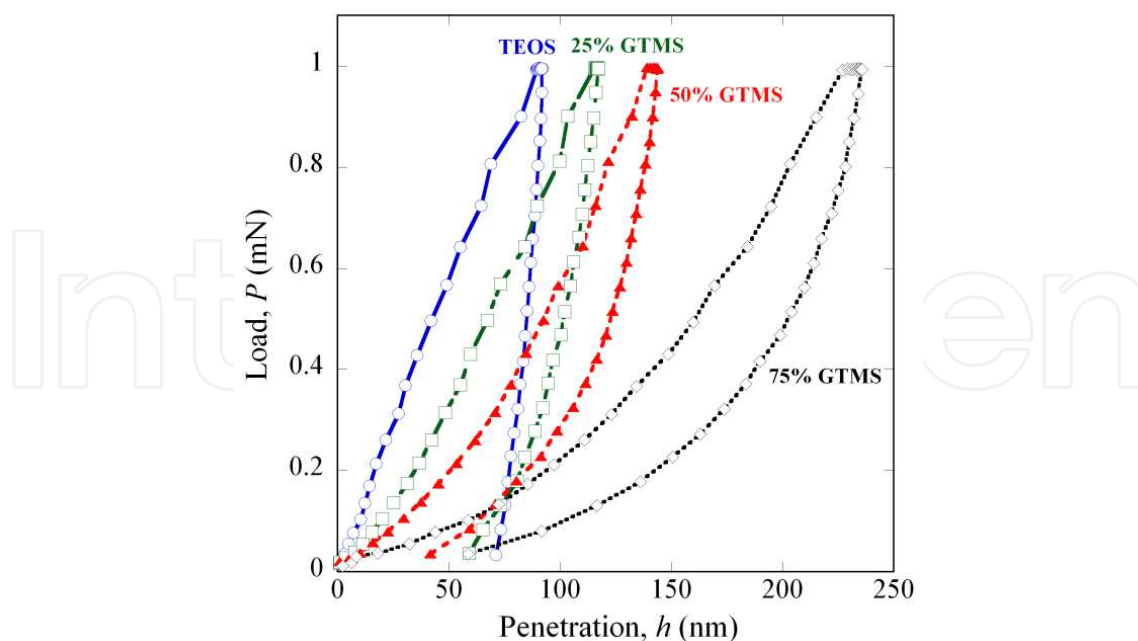
Figure 8. Indentation load-displacement curves for TEOS and GTMS on Cu substrates. $P = 1$ mN with 10 s dwell at maximum force [Redrawn from ref (Latella et al., 2008a)].
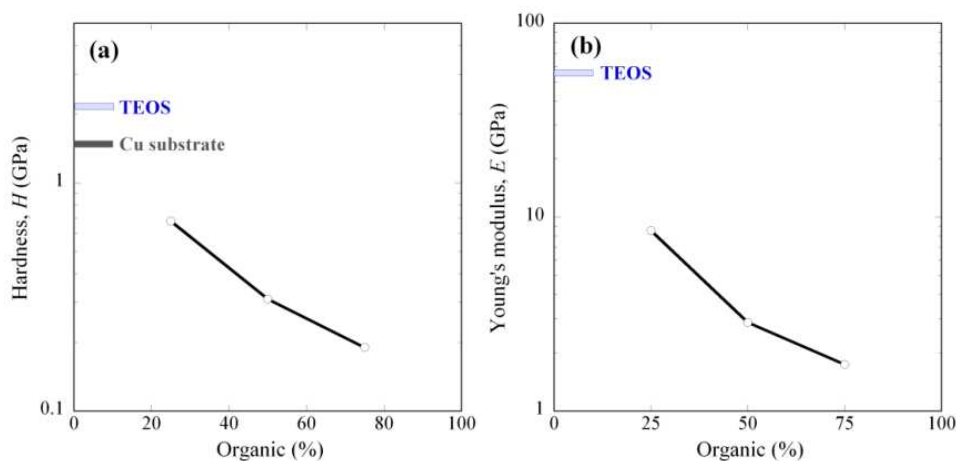

Figure 9. Plots of (a) Hardness and (b) Young's modulus of the GTMS coatings versus percentage organic addition. Hatched boxes at the right correspond to the properties of the TEOS coating and the Cu substrate (not shown is $E_{Cu} \approx 120$ GPa) [From ref (Latella, 2008b)].

Figure 10(a) shows the creep data for the TEOS and the three GTMS films. Creep penetration as a function of time, taken from five indents at each hold time, for the various coatings was examined using step loading (Oyen, 2005) to $P_{max} = 0.5$ mN for a 90 s hold with the 1 μm spherical indenter. Examples of the best fit curves of various spring-dashpot models (see section 3.3.2) for the 50% and 75% GTMS films are shown in Figure 10(b). The results from the fitting of the creep curves using the three- and four-element mechanical models for all coatings are presented in Table 1. Noting that the E values quoted were corrected from the best-fit parameters (E'): $E'(1-v_m^2)$. Figure 10(a) shows clearly the effect of the organic addition resulted in films with increased creep behaviour compared to the

baseline inorganic TEOS film. Furthermore the initial penetration and creep deformation escalated substantially with the increasing level of the GTMS addition. Comparing the E_1 and η_1 values for the spring-dashpot models of the materials, the trend is for Young's modulus and viscosity to decrease with increasing level of organic in accord with the trends observed in the mechanical property results. There was little difference in the E_1 values obtained using the three-element and four-element models although there is some discrepancy with the values obtained using the indentation load-partial unload method of analysis (Latella et al., 2008a). Clearly a three-element model is sufficient for extracting the key material parameters of these films even though slightly better fits using four adjustable parameters are obtained in some instances based on the R^2 values. Irrespective of model the standard error for each parameter ranged from 0.2% to a maximum of 5%.
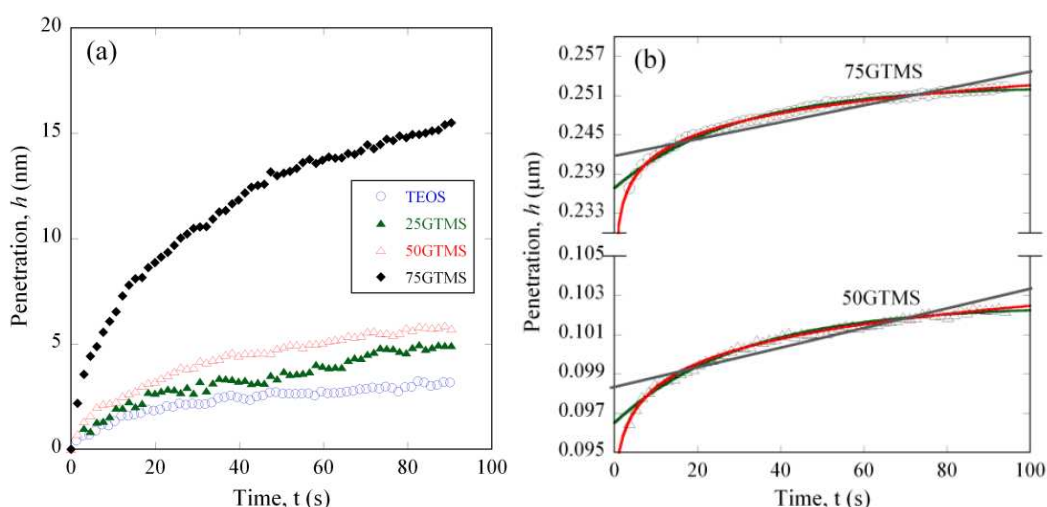

Figure 10. (a) Creep curves corrected for initial penetration for GTMS films. TEOS data is shown in both for comparison. Step loading to $P = 0.5$ mN for 90 s. (b) Examples of fits to raw creep data of the 50% GTMS and 75% GTMS. Solid lines are fits from Maxwell (grey), three-element (green) and logarithmic equations (red) [Redrawn from ref (Latella et al., 2008a)].

	TEOS	25% GTMS	50% GTMS	75% GTMS
Three-element model				
E_1 [GPa]	35.3	21.8	11.7	3.06
E_2 [GPa]	354	174	132	32
η_1 [GPa s]	8814	10178	4045	945
R^2	0.97	0.95	0.99	0.99
Four-element model				
E_1 [GPa]	36.0	22.8	11.8	3.10
E_2 [GPa]	436	323	186	44
η_1 [GPa s]	85974	27139	30715	8035
η_2 [GPa s]	4958	2267	2632	624
R^2	0.98	0.98	0.99	0.99

Table 1. Creep fit parameters for the TEOS and GTMS films.

SEM images of cracking behaviour from microtensile tests of the TEOS and 50% GTMS films on the copper are shown in Figures 11 and 12. The tests have been made at a common imposed total strain of ≈15%. For the TEOS film (Fig. 11(a)) regularly spaced parallel cracks in the coating layer perpendicular to the tensile axis are evident and normal to the interface (loading direction is horizontal) that appear throughout the entire gauge length of the specimen. These cracks multiply in number with increasing elongation leading to a decrease in the crack spacing to a saturation level with no further cracking i.e. intercracking distance of ≈ 5 μm. Fig. 11(b) shows a higher magnification image of a region in the coating that is heavily delaminated from the Cu substrate. These localised debonded zones vary in size with some buckled and fractured fragments evident between parallel cracks. The damage in the 50% GTMS film is shown in Figure 12. In stark contrast to the TEOS film, short cracks scattered throughout the coating are apparent (Fig. 12(a)). It shows excellent coating–substrate adhesive bonding (Fig. 12(b)). Some areas of the coating are free from cracking and there is negligible debonding, which can be attributed to the viscoelastic behaviour of the GTMS film. The difference in the cracking behaviour of the coatings is consistent with the nanoindentation tests, confirming a brittle to viscoelastic change in mechanical response due to the addition of the long-chained GTMS species.
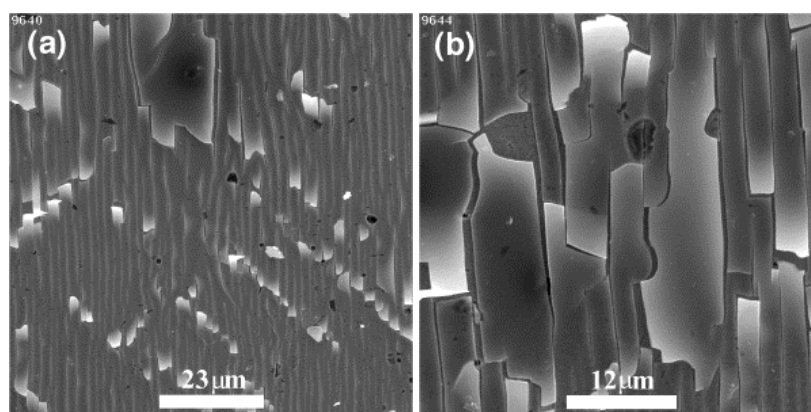

Figure 11. SEM images of cracking and debonding in the TEOS sol-gel film on Cu after tensile testing (15% total strain) showing (a) overall cracking and (b) small cracks.
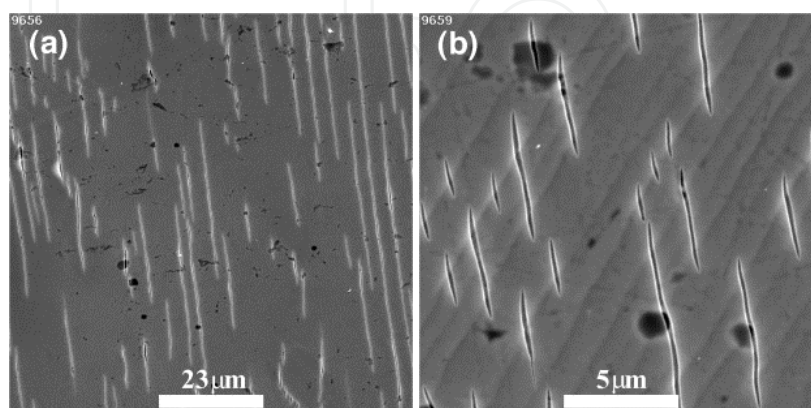

Figure 12. SEM images of cracking in the 50% GTMS sol-gel film on Cu after tensile testing (15% total strain) showing (a) overall cracking and (b) small cracks. Note the absence of debonding in GTMS compared to TEOS (Fig. 11). Tensile axis is horizontal in all images.

From the tensile tests the first signs of coating separation from the substrate observed as buckling in the optical microscope, irrespective of the deadhesion size or extent, was the criterion used for ascertaining the strain for debonding. The critical strains for debonding, ε_d, of the TEOS and the 50% GTMS films from the Cu substrates observed in the tensile tests are presented in Table 2 along with the apparent interfacial fracture energy (see equation 22). Because of the viscoelastic nature of the 50% GTMS film, the irregular nature of cracking and the absence of debonding, the interface fracture energy is a lower-bound estimate given that the calculation assumes linear elastic behaviour. The tensile strain required for debonding clearly shows that higher strains are required to generate debonding in the 50% GTMS film compared to TEOS. The interfacial energy for TEOS of 22 Jm^{-2} appears reasonable given that the fracture energy of soda-lime glass is $\gamma \approx 10$ Jm^{-2}. In the absence of debonding in the 50% GTMS film at a strain of 15% the interfacial fracture energy is clearly much greater than 14.5 Jm^{-2}.

	TEOS (0% GTMS)	50% GTMS
Critical applied strain for film debonding, ε_d [%]	6.5	>15
Apparent interfacial fracture energy, γ_i [Jm^{-2}]	22	>> 14.5

Table 2. Debonding parameters from tensile testing of the TEOS and 50% GTMS films on Cu substrates.

5.3. Case study 3 – Similar chain length and polymerisation

5.3.1. Similar chain length

To study the influence of the nature of the organic substituent on the mechanical properties of the hybrid film, GTMS was substituted by different organotrialkoxysilanes with similar chain lengths. All solutions were prepared at pH=2 with an equivalent SiO$_2$ concentration of 5 wt% and aged for 24 h at room temperature. A mixture of 50% TEOS and 50% organic: n-[3-(trimethoxysilyl)propyl]ethylene diamine (designated TMOSPEDA), n-octyltrimethoxysilane (designated OTES) were prepared. The GTMS film was prepared using THF (to avoid ring opening – see section 5.3.2) whereas ethanol was used as the solvent for TMOSPEDA and OTES. Various parameters in the preparation of the films could not be easily controlled. For example TMOSPEDA hydrolyses very quickly so the rate of hydrolysis between the samples was not the same for a given ageing time. The morphology and the roughness of the spin-coated sol-gel films on Si wafers were quite different as shown in Figure 13. The GTMS film is smooth and featureless whereas TMOSPEDA is striated and OTES results in a non-uniform coating with many pinholes.
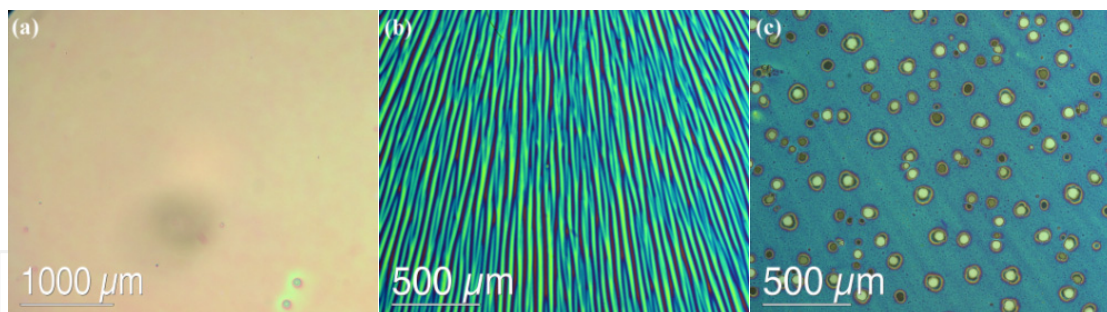
Figure 13. Optical micrographs of spin coated surfaces (a) GTMS (thickness, t = 590 nm), (b) TMOSPEDA (t = 270 nm) and (c) OTES (t = 320 nm).

Figure 14 show Young's modulus for the three sol-gel films with different end group precursors from indentations, away from pinholes and striations, on the solid phase of the films where applicable. The GTMS film has the higher modulus followed by TMOSPEDA and then OTES. The same trend in hardness is also observed. The data indicates better network connectivity in the GTMS structure compared to TMOSPEDA and OTES.
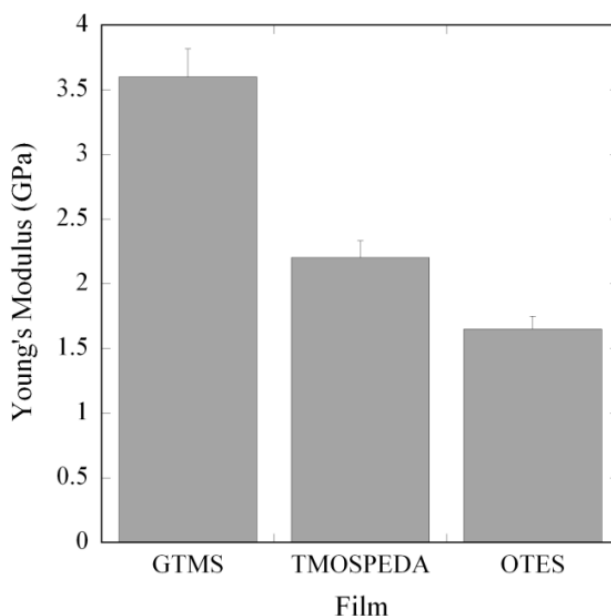

Figure 14. Young's modulus of the hybrid sol-gel films with similar chain lengths deposited on Si wafers.

Although not shown the tensile testing experiments agree with the nanoindentation results with the film strength following the same trend: GTMS (σ_c = 45 MPa), TMOSPEDA (σ_c = 40 MPa) and OTES (σ_c = 22 MPa) but interface fracture energy for the lower modulus and lower strength films is improved. Likewise the film damage studies indicated less delamination failures of these softer films, which were expected as they are more compliant, deformable and exhibit viscoelastic tendencies which provides greater resilience to fracture. Hence these types of soft films yield larger cohesive zones under externally applied stresses inhibiting catastrophic interfacial cracking and debonding as opposed to more brittle coatings (*cf.* Figs. 11 and 12).

5.3.2. Polymerisation

The previous case studies have illustrated that GTMS is commonly used as an organometallic precursor in organic-inorganic hybrid coatings because of its ability to undergo both hydrolysis-polycondensation (through the trialkoxysilyl group) and organic polymerisation by ring opening of the terminal epoxy group. Such features make GTMS a very attractive compound for the fabrication of hybrid co-polymers where the organic chains and the inorganic tridimensional network are interpenetrated, by provoking the hydrolysis and the ring opening polymerisation either simultaneously or in a controlled two-step process. To investigate the effects of ring opening in GTMS, samples were prepared using the same sol-gel chemistry as described above but here the solvents ethanol and THF were compared. The coatings produced ranged from 600 to 700 nm in thickness. In ethanol, it was determined by ^{13}C NMR that 10% of the ring was opened after 1 day at room temperature and 60% after 3 days at 60°C. The corresponding samples in THF after 1 day at room temperature showed no consequent ring opening and 10% opening after 3 days at 60°C.

Figure 15 compares the Young's modulus and hardness of the coatings resulting from GTMS sols prepared in either ethanol or THF and aged for different times. This allowed an estimation of the effect of the ring cleavage, without polymerisation, on the mechanical properties of the hybrid film. One consideration was that the presence of alcohol or ether groups at the end of the organic chain could allow some connectivity with the inorganic network through sol-gel type reactions with silanols or strong hydrogen bonding, thus improving the overall strength of the film (Metroke et al., 2002). The results showed that samples aged under the same conditions presented similar mechanical responses. More interestingly, a pronounced difference was observed between samples aged for 1 day at room temperature and those aged 3 days at 60°C. While the expected result was an increase of the Young's modulus with an increase of the silica network condensation, the opposite result was observed.

The presence of long organic chains in the precursor sol appears to reduce the long range connectivity of the inorganic network. This nano-segregation affects the overall cohesion of the hybrid coating and its mechanical strength drops with prolonged ageing. This emphasises the importance of cross-polymerisation of the organic groups in the film to maintain a strong interpenetrated network. This is further reinforced by the tensile testing results as illustrated in Figure 16. The 0% ring opened film shows extensive damage and delamination (Fig. 16(a)). By contrast the adhesion behaviour of the 10% ring opened film (Fig. 16(b)) is better with small cracks and debonded regions – typical of the standard GTMS film behaviour (see sections 5.1 and 5.2). In the 60% ring opened film (3 day aged at 60°C), there is slightly more debonding than the 10% ring opened film but the cracking is rather more irregular similar to a tearing appearance.

Opening of the epoxy ring in GTMS during the sol-gel process does not influence significantly the mechanical properties, for the same ageing time. Although when GTMS is

allowed to reach higher hydrolysis-polycondensation states, i.e. longer ageing times, the mechanical properties of the coatings are degraded significantly and the surface roughness is increased. Figure 17 shows the strength, film toughness and interfacial fracture energy for the coatings. Again the same trends are apparent with nano-segregation between the organic and inorganic part of the hybrid presumably responsible for the decrease in strength, toughness and adhesion of the film with ageing time.
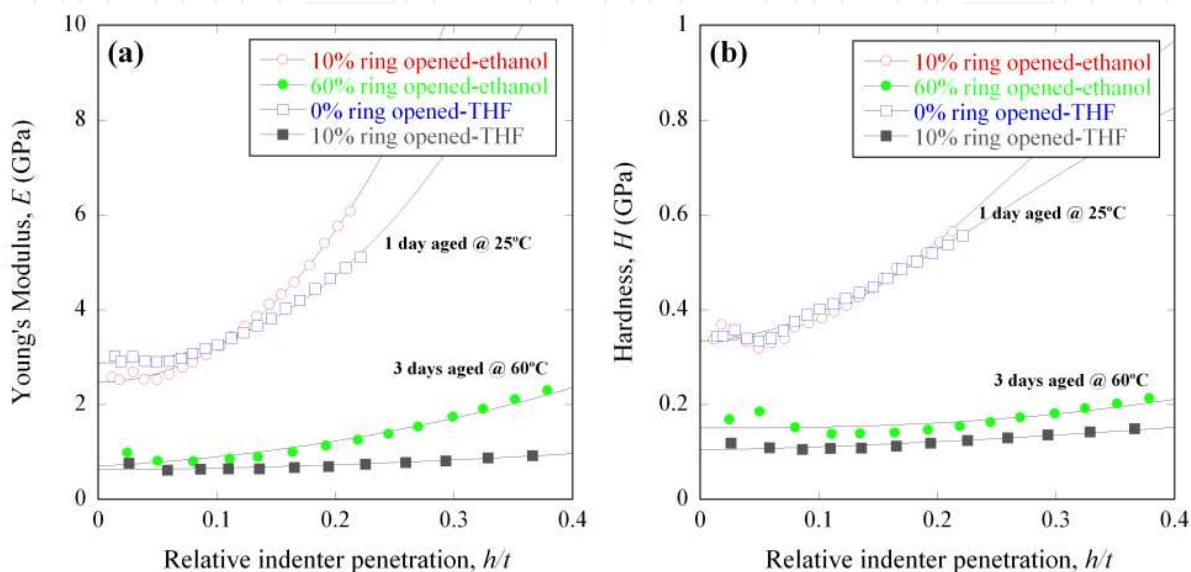

Figure 15. Plots of (a) Young's modulus and (b) hardness as a function of relative indenter penetration (depth to thickness, h/t) of the GTMS films at specific ageing time and temperature. Indicated is the amount of ring opening of the structure – for the THF based sols there is 0% and 10% ring opening but for ethanol based sols there is 10% and 60% ring opening. Solid lines are fits to the data using the method in ref (Jung et al., 2004).
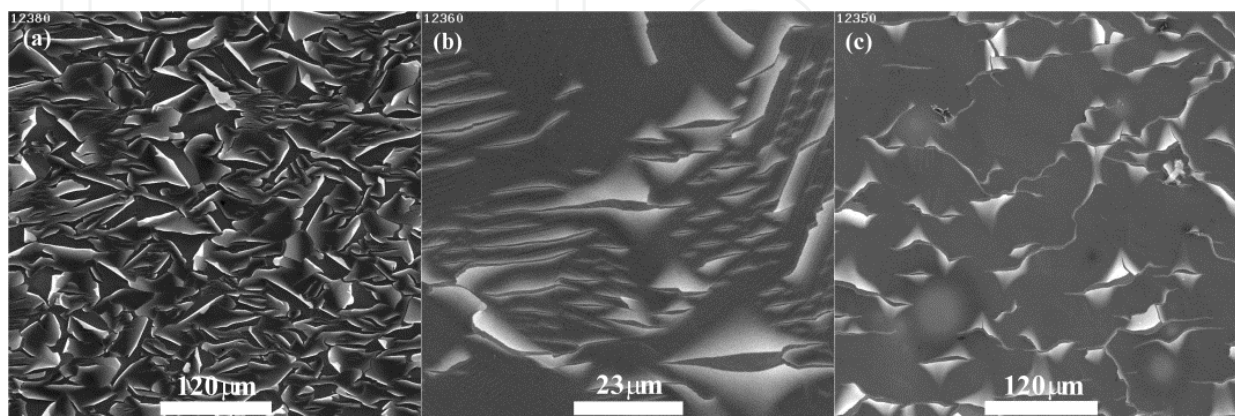

Figure 16. SEM images of damage in GTMS films on stainless steel after tensile testing: (a) 0% ring opening (THF-1 day aged at 25°C), (b) 10% ring opening (ethanol-1 day aged at 25°C) and (c) 60% ring opening (ethanol-3 days aged at 60°C). Tensile axis is vertical in these images.
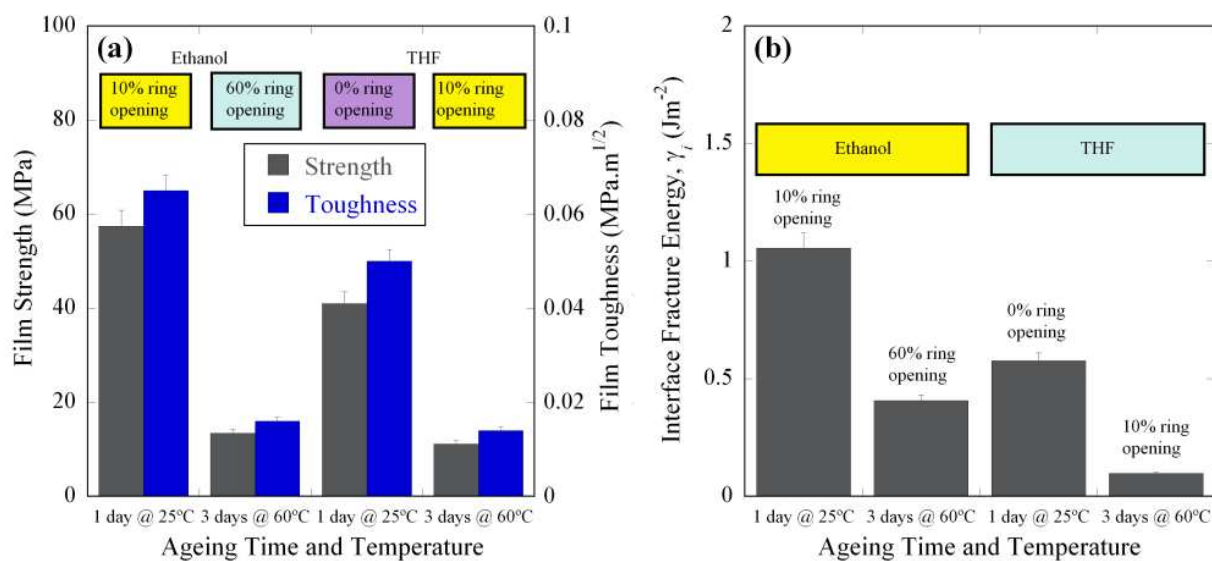
Figure 17. (a) Strength and fracture toughness and (b) interfacial fracture energy of the GTMS thin film coatings at specific ageing time and temperature. Also indicated is the amount of ring opening of the structure – for the THF based sols there is 0% and 10% ring opening but for ethanol based sols there is 10% and 60% ring opening.

6. Conclusion

The approach described in this chapter using both instrumented nanoindentation and micromechanical tensile testing provides significant insights into the effects of organic substituent (type/quantity) in these hybrid thin film systems regarding their mechanical and adhesion behaviour. The advantages of using nanoindentation for thin film characterisation are widely known and the work surveyed here has shown that its flexibility can be used to extract intrinsic film properties and also qualitatively provide insights on film attributes from load-displacement responses. Tensile testing is a practical complementary tool as it provides qualitative and quantitative appreciation of film fracture and damage evolution under controlled strains. Likewise, intrinsic film properties and interfacial adhesion energies can be extracted from *in-situ* experiments. The application of these techniques has been demonstrated on model sol-gel hybrid films with the following key findings:

1. Film properties and adhesion behaviour are dramatically affected by the nature of the organometallic precursors. Shorter chain length gives rise to higher Young's moduli. Smaller differences are observed between precursors with similar chain length but different functionality.
2. GTMS films on a variety of substrates exhibit excellent adhesion and minimal damage under external loading. The modifying ability of the long-chained GTMS molecule affects the network structure to such an extent resulting in viscoelastic flow and relaxation processes to occur under contact and external loading similar to those commonly seen in polymeric materials.
3. The balance between mechanical rigidity and adhesion is dependent on the proportion of $Si(OR)_4$ used in the hybrid films.

4. The epoxy ring opening in GTMS films did not influence the mechanical behaviour of the film to any great extent suggesting that polymerisation did not proceed.
5. Ageing of the hybrid sols for extended times resulted in a dramatic drop in mechanical properties.

Author details

Bruno A. Latella
Commonwealth Science and Industrial Research Organisation, WA, Australia

Michael V. Swain
Biomaterials Science, Faculty of Dentistry, University of Sydney, NSW, Australia

Michel Ignat
Physics Department, School of Engineering, University of Chile, Beauchef, Santiago, Chile

Acknowledgement

7. References

Agrawal, D.C. & Raj, R. (1989). Measurement of the ultimate shear-strength of a metal ceramic interface. *Acta Metallurgica,* 37(4) pp. 1265-1270.

Atanacio, A.J., Latella, B.A., Barbé, C.J. & Swain, M.V. (2005). Mechanical properties and adhesion characteristics of hybrid sol-gel thin films. *Surface and Coatings Technology,* 192(2-3) pp. 354-364.

Beake, B. (2006). Modelling indentation creep of polymers: a phenomenological approach. *Journal of Physics D: Applied Physics,* 39 pp. 4478-4485.

Berthoud, P., Sell, C.G. & Hiver, J-M. (1999). Elastic-plastic indentation creep of glassy poly(methyl methacrylate) and polystyrene: characterisation using uniaxial compression and indentation. *Journal of Physics D: Applied Physics,* 32 pp. 2923-2932.

Beuth, J.L. & Klingbeil, N.W. (1996). Cracking of thin films bonded to elastic-plastic substrates. *Journal of Mechanics and Physics of Solids,* 44(9) pp. 1411-1428.

Bland, D.R. (1960). *Theory of Linear Viscoelasticity.* Pergamon, Oxford.

Brinker, C.J. & Scherrer, G.W. (1990). *Sol-Gel Science: The Physics and Chemistry of Sol-Gel Processing.* Academic Press, San Diego.

Chudoba, T. & Richter, F. (2001). Investigation of creep behaviour under load during indentation experiments and its influence on hardness and modulus results. *Surface and Coatings Technology,* 148(2-3) pp. 191-198.

Field, J.S. & Swain, M.V. (1993). A simple predictive model for spherical indentation. *Journal of Materials Research*, 8(2) pp. 297-306.

Field, J.S. & Swain, M.V. (1995). Determining the mechanical properties of small volumes of material from submicrometer spherical indentations. *Journal of Materials Research*, 10(1) pp. 101-112.

Filiaggi, M.J., Pilliar, R.M. & Abdulla, D. (1996). Evaluating sol-gel ceramic thin films for metal implant applications. II. Adhesion and fatigue properties of zirconia films on Ti-6Al-4V. *Journal of Biomedical Materials Research*, 33(4) pp. 239-256.

Fischer-Cripps, A.C. (2002). *Introduction to Nanoindentation*. Springer, New York.

Fischer-Cripps, A.C. (2004). A Simple phenomenological approach to nanoindentation creep. *Materials Science and Engineering A*, 385 pp. 74-82.

Haas, K.H. & Wolter, H. (1999). Synthesis, properties and applications of inorganic-organic copolymers (ORMOCER®s). *Current Opinion in Solid State and Materials Science*, 4 pp. 571-580.

Haas, K.H., Amberg-Schwab, S. & Rose, K. (1999a). Functionalised coating materials based on inorganic-organic polymers. *Thin Solid Films*, 351(1-2) pp. 198-203.

Haas, K.H., Amberg-Schwab, S., Rose, K. & Schottner, G. (1999b). Functionalized coatings based on inorganic-organic polymers (ORMOCER®s) and their combination with vapor deposited inorganic thin films. *Surface & Coatings Technology*, 111(1) pp. 72-79.

Haq, A., Munroe, P.R., Hoffman, M., Martin, P.J. & Bendavid, A. (2010). Effect of coating thickness on the deformation behaviour of diamond-like carbon-silicon system. *Thin Solid Films*, 518(8) pp. 2021-2028.

Harry, E., Ignat, M., Pauleau, Y., Rouzard, A. & Juliet, P. (2000). Mechanical behaviour of hard PVD multilayered coatings. *Surface and Coatings Technology*, 125(1-3) pp. 185-189.

He, L.H., Standard, O.C., Huang, T.T.Y., Latella, B.A. & Swain, M.V. (2008). Mechanical behaviour of porous hydroxyapatite. *Acta Biomaterialia*, 4(3) pp. 577-586.

He, L.H. & Swain, M.V. (2009). Nanoindentation creep behavior of human enamel. *Journal of Biomedical Materials Research Part A*, 91(2) pp. 352-359.

Hertz, H. (1896). *Hertz's Miscellaneous Papers*. Chs. 5,6. Macmillan, London.

Hu, M.S. & Evans, A.G. (1989). The cracking and decohesion of thin films on ductile substrates. *Acta Metallurgica*, 37(3) pp. 917-925.

Ignat, M. (1996). Mechanical response of multilayers submitted to in-situ experiments. *Key Engineering Materials*, 116-117 pp. 279-290.

Ignat, M., Marieb, T., Fujimoto, H. & Flinn, P.A. (1999). Mechanical behaviour of submicron multilayers submitted to microtensile experiments. *Thin Solid Films*, 353(1-2) pp. 201-207.

Innocenzi, P., Esposto, M. & Maddalena, A. (2001). Mechanical properties of 3-glycidoxypropyltrimethoxysilane based hybrid organic-inorganic materials. *Journal of Sol-Gel Science and Technology*, 20(3) pp. 293-301.

Jung, Y.-G., Lawn, B.R., Martyniuk, M., Huang, H. & Hu, X.Z. (2004). Evaluation of elastic modulus and hardness of thin films by nanoindentation. *Journal of Materials Research*, 19(10) pp. 3076-3080.

Kumar, M.V.R. & Narasimhan, R. (2004). Analysis of spherical indentation of linear viscoelastic materials. *Current Science,* 87(8) pp. 1088-1095.

Latella, B.A., Ignat, M., Barbé, C.J., Cassidy, D.J. & Bartlett, J.R. (2003). Adhesion behaviour of organically-modified silicate coatings on stainless steel. *Journal of Sol-Gel Science and Technology*, 26(1-3) pp. 765-770.

Latella, B.A., Ignat, M., Barbé, C.J., Cassidy, D.J. & Li, H. (2004). Cracking and decohesion of sol-gel hybrid coatings on metallic substrates. *Journal of Sol-Gel Science and Technology*, 31(1-3) pp. 143-149.

Latella, B.A., Triani, G., Zhang, Z., Short, K.T., Bartlett, J.R. & Ignat, M. (2007a). Enhanced adhesion of atomic layer deposited titania on polycarbonate substrates. *Thin Solid Films,* 515(5) pp. 3138-3145.

Latella, B.A., Ignat, M., Triani, G., Cassidy, D.J. & Bartlett, J.R. (2007b). Fracture and Adhesion of Thin Films on Ductile Substrates. In: A*dhesion Aspects of Thin Films, Volume 3*, Mittal, K.L., pp. 47-57, VSP, Leiden.

Latella, B.A., Gan, B.K., Barbé, C.J. & Cassidy, D.J. (2008a). Nanoindentation hardness, Young's modulus, and creep behavior of organic-inorganic silica-based sol-gel thin films on copper. *Journal of Materials Research,* 23(9) pp. 2357-2365.

Latella, B.A. (2008b). Indentation creep and adhesion of hybrid sol-gel coatings. *Advanced Materials Research,* 41-42 pp. 305-311.

Lawn, B.R. (1998). Indentation of ceramics with spheres: a century after Hertz. *Journal of the American Ceramic Society*, 81(8) pp. 1977-1994.

Lee, E.H. & Radok, J.R.M. (1960). The contact problem for viscoelastic bodies. *Journal of Applied Mechanics*, 27 pp. 438-444.

Letailleur, A., Ribot, F., Boissiere, C., Teisseire, J., Barthel, E., Desmazieres, B., Chemin, N. & Sanchez, C. (2011). Sol-gel derived hybrid thin films: the chemistry behind processing. *Chemistry of Materials*, 23(22) pp. 5082-5089.

Lucas, B. & Oliver, W. (1999). Indentation power-law creep of high-purity indium. *Metallurgical and Materials Transactions A-Physical Metallurgy and Materials Science* 30(3) pp. 601-610.

Mackenzie, J.D. (1994). Structures and properties of ormosils. *Journal of Sol-Gel Science and Technology*, 2(1-3) pp. 81-86.

Mackenzie, J.D. & Bescher, E. (1998). Structures, properties and potential applications of Ormosils. *Journal of Sol-Gel Science and Technology*, 13(1-3) pp. 371-377.

Mackenzie, J.D. & Bescher, E. (2000). Physical properties of sol-gel coatings. *Journal of Sol-Gel Science and Technology,* 19(1-3) pp. 23-29.

Mackenzie, J.D. & Bescher, E. (2003). Some factors governing the coating of organic polymers by sol-gel derived hybrid materials. *Journal of Sol-Gel Science and Technology,* 27(1) pp. 7-14.

Malzbender, J., den Toonder, J.M.J., Balkenende, A.R. & de With, G. (2002). Measuring mechanical properties of coatings: a methodology applied to nano-particle-filled sol-gel coatings on glass. *Materials Science & Engineering R-Reports,* 36(2-3) pp. 47-103.

Mammeri, F., Le Bourhis, E., Rozes, L. & Sanchez, C. (2005). Mechanical properties of hybrid organic-inorganic materials. *Journal of Materials Chemistry*, 15(35-36) pp. 3787-3811.

Metroke, T.L., Parkhill, R.L. & . Knobbe, E.T. (2001). Passivation of metal alloys using sol-gel derived materials – a review. *Progress in Organic Coatings,* 41 pp. 233-238.

Metroke, T.L. Kachurina, O. & Knobbe, E.T. (2002). Spectroscopic and corrosion resistance characterization of GLYMO-TEOS ormosil coatings for aluminum alloy corrosion inhibition. *Progress in Organic Coatings,* 44(4) pp. 295-305.

Oliver, W.C. & Pharr, G.M. (1992). An improved technique for determining hardness and elastic modulus using load and displacement sensing indentation experiments. *Journal of Materials Research*, 7(6) pp. 1564-1573.

Oyen, M.L. (2005). Spherical indentation following ramp loading. *Journal Of Materials Research*, 20(8) pp. 2094-2100.

Oyen, M.L. (2006). Analytical techniques for indentation of viscoelastic materials. *Philosophical Magazine,* 86(33-35) pp. 5625-5641.

Roest, R., Latella, B.A., Heness, G. & Ben-Nissan, B. (2011). Adhesion of sol-gel derived hydroxyapatite nanocoatings on anodised pure titanium and titanium (Ti6Al4V) alloy substrates. *Surface and Coatings Technology*, 205(11) pp. 3520-3529.

Samson, F. (1996). Ophthalmic lens coatings. *Surface and Coatings Technology*, 81(1) pp. 79-86.

Sanchez, C., Julian, B., Belleville, P. & Popall, M. (2005). Applications of hybrid organic-inorganic nanocomposites. *Journal of Materials Chemistry*, 15(35-36) pp. 3559-3592.

Scafidi, P. & Ignat, M. (1998). Cracking and loss of adhesion of Si_3N_4 and SiO_2:P films deposited on Al substrates. *Journal of Adhesion Science and Technology*, 12(11) pp. 1219-1242.

Schmidt, H. (1985). New type of non-crystalline solids between inorganic and organic materials. *Journal of Non-Crystalline Solids*, 73 pp. 681.

Schottner, G. (2001). Hybrid sol-gel-derived polymers: Applications of multifunctional materials. *Chemistry of Materials,* 13(10) pp. 3422-3435.

Volinsky, A., Vella, J.B. & Gerberich, W.W. (2003). Fracture toughness, adhesion and mechanical properties of low-k dielectric thin films measured by nanoindentation. *Thin Solid Films*, 429(1-2) pp. 201-210.

Wang, J.S., Sugimura, Y., Evans, A.G. & Tredway, W.K. (1998). The mechanical performance of DLC films on steel substrates. *Thin Solid Films*, 325(1-2) pp. 163-174.

Wen, J. & Wilkes, G. (1996). Organic/inorganic hybrid network materials by the sol-gel approach. *Chemistry of Materials*, 8(8) pp. 1667-1681.